Journal of Hydrology 590 (2020) 125224

Contents lists available at ScienceDirect

Journal of Hydrology

journal homepage: www.elsevier.com/locate/jhydrol

Research papers

The electroviscous flow of non-Newtonian fluids in microtubes and implications for nonlinear flow in porous media

Zhilin Cheng[a,b,*], Zhengfu Ning[a], Sheng Dai[b]

[a] State Key Laboratory of Petroleum Resources and Prospecting, China University of Petroleum, Beijing 102249, China
[b] School of Civil and Environmental Engineering, Georgia Institute of Technology, Atlanta 30332, GA, USA

ARTICLE INFO

This manuscript was handled by Huaming Guo, Editor-in-Chief, with the assistance of WeiCheng Lo, Associate Editor

Keywords:
Non-Newtonian
Electroviscous flow
Microtubes
Low-velocity nonlinear flow

ABSTRACT

This paper aims to interpret the low-velocity nonlinear flow occurring in low-permeability reservoirs based on the theories of electrokinetic transport and non-Newtonian rheology of fluids. To achieve this end, we simulate the steady-state electroviscous flow of Bingham-Papanastasiou (BP) fluids in circular microtubes by simultaneously solving the Poisson-Boltzmann and the modified Navier-Stokes equations. The induced electrical field strength $|E_s|$, velocity profiles, and the transport capacity of the non-Newtonian fluid under the effects of various factors (such as capillary radius R, zeta potential ζ, yield stress τ_0, and stress growth index m) were examined. The results show that the generated $|E_s|$ of the BP fluid is highly affected by the fluid rheology, which is quite different from that of the Newtonian liquid. The velocity profiles become lower and flatter as m or τ_0 increases, and this is more remarkable in smaller microtubes. The apparent viscosity of non-Newtonian fluid declines monotonically with increasing c_∞, yet non-monotonically with R, m, τ_0, and ζ. In addition, the low-velocity nonlinear flow in microtubes can be successfully captured when considering the electrokinetic flow of the non-Newtonian fluid rheology. While for the Newtonian fluid, only involving the electroviscous effect fails to generate the nonlinear flow behavior. The contributions of electrokinetic parameters versus rheological properties to the degree of flow nonlinearity are also discussed. The impact of electrokinetic parameters (ζ, c_∞) on the flow characteristics is significant at high-pressure gradients and becomes trivial when the pressure gradient is relatively low. In contrast, the fluid rheological parameters (m, τ_0) greatly determine the magnitude of the flow nonlinearity occurring at the low-pressure gradients. In sum, the electroviscous flow of BP fluids in microchannels provides a possible explanation of the low-velocity non-Darcy flow in porous media.

1. Introduction

Fluid flow in porous media is often described by Darcy's law, which characterizes a linear correlation between flow velocity and the pressure gradient (Bear, 2013; Kumar et al., 2020). However, numerous studies (Soni et al., 1978; Coles and Hartman, 1998; Dejam et al., 2017; Diwu et al., 2018) have shown that the Darcy velocity, in both saturated and unsaturated flows, exhibits nonlinear dependence on the pressure gradient in low permeability porous media at low pressure gradients, as illustrated in Fig. 1a. This nonlinear behavior may result from strong liquid-solid interactions in a thin layer close to the solid surface due to the combined effects of various interfacial forces. Whether these forces require a threshold pressure gradient (TPG) to initiate the flow is still debatable (Wei et al., 2009; Wang and Sheng, 2017). The direct measurement of the TPG is often not practical since the flow rate in low permeable media is always too low to be accurately determined. In fact, the TPG value is generally obtained by fitting experimental data with considerable uncertainties. Nevertheless, whether the TPG exists remains unanswered to date, while the low-velocity non-Darcian flow in low permeability porous media is widely recognized (Liu et al., 2012).

To characterize the nonlinear flow in porous media, extensive experiments have been conducted using fluids like tap water, deionized water, or various formation liquids. These experimental data allow establishing correlations to describe the nonlinear feature of the flow in porous samples (Prada and Civan, 1999; Hao et al., 2008; Zeng et al., 2011). An earlier work by Miller and Low (1963) observed the TPG as a result of water-clay interaction when water flows through different clayey specimens. Prada and Civan (1999) performed a series of brine flow tests through sandstones and sandpack samples and proposed a modified Darcy's law that the flow velocity is proportional to a power relation of the pressure gradient. Additionally, Zeng et al. (2011) measured the velocity-gradient curves for various types of fluids

* Corresponding author at: State Key Laboratory of Petroleum Resources and Prospecting, China University of Petroleum, Beijing 102249, China.
E-mail address: zhilin_cheng1992@163.com (Z. Cheng).

https://doi.org/10.1016/j.jhydrol.2020.125224
Received 5 April 2020; Received in revised form 14 June 2020; Accepted 22 June 2020
Available online 06 July 2020
0022-1694/

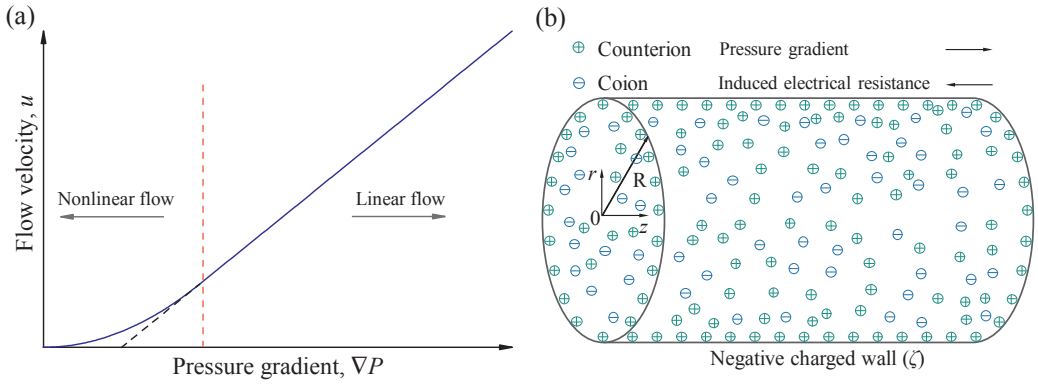

Fig. 1. (a) The velocity-gradient curve for low-velocity nonlinear flow; (b) Schematic of the electrokinetic flow of fluids in a capillary.

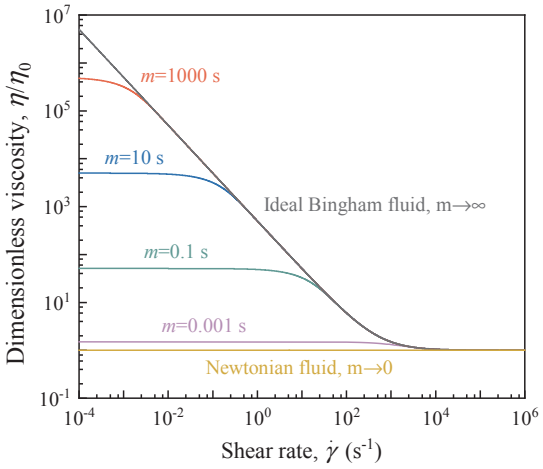

Fig. 2. The dimensionless shear viscosity η/η_0 versus the shear rate $\dot{\gamma}$ for various values of m, calculated using Eq. (2). The fixed parameters areη_0 = 1 mPa·s andτ_0 = 0.5 Pa.

flowing through ultra-low permeability rocks and obtained empirical relations between the TPG and sample permeability. Recently, by critically reviewing the current advances and discussing the nonlinear flow mechanisms, Wang and Sheng (2017) used the boundary-layer theory (Huang et al., 2013) (including the boundary and bulk fluid, shown in Fig. 2 of their work) to describe the nonlinear flow mechanism. However, a universal mechanism responsible for the nonlinear seepage phenomenon in reservoirs remains elusive.

An enhanced understanding of the underlying mechanisms of nonlinear flow in tight porous media is of great societal and economic interests, in the context of the exploration of unconventional reservoirs such as shale gas and tight oil. Fluid flow in such tight porous media is typically subjected to low pressure gradients and exhibits strong non-Darcian behavior (Diwu et al., 2018). This non-Darcy flow highly affects the well production and the injection operation in tight reservoirs (Chen et al., 2017). Therefore, to uncover the underlying mechanics of non-Darcian behaviors of fluids becomes crucial to the successful development of unconventional resources. However, such reservoir rocks mainly contain micro- and nano-scale pores (Loucks et al., 2009; Zhao et al., 2015; Cheng et al., 2019), which precludes the accuracy of conventional core flooding experiments, as mentioned above. On the other hand, the rapid development of microelectromechanical technology provides an alternative approach to study the diverse physical phenomena, such as microfluidic mixing (Kirby, 2010), heat transfer (Ayoubloo et al., 2019; Ghalambaz et al., 2019; Shashikumar et al., 2019), and fluid flow at the microscale (Li, 2004; Masliyah and Bhattacharjee, 2006). For instance, authors (Wang et al., 2009; Yang et al., 2011; Wu et al., 2017a,b) have performed flow experiments using micro-fluidic channels to study the novel features of micro-scale flow. It has been shown that the observed nonlinear flow at low pressure gradient can be explained by the boundary-layer theory, assuming the adsorption of polarized water molecules on hydrophilic solid surfaces; and the thickness of the boundary-layer decreases with increased pressure gradient until a certain thickness cannot be reduced any further even at a higher pressure gradient (Wu et al., 2017a).

The impact of surface-dominated forces in microfluidics originating from the liquid-wall interaction on the flow becomes indispensable when the flow channels are at the micro- and nano-scales (Brutin and Tadrist, 2003). One of the surface-dominated forces arises from the electrical double layer (EDL) effect (Hunter, 1981; Li, 2004). EDL is essentially a physical structure that spontaneously appears on a solid surface when it is in contact with an electrolyte solution. An electrical potential difference at the solid-liquid interface leads to the rearrangement of ions within the EDL. In the presence of an external pressure gradient, the solution transport in microfluidics can be greatly influenced by the electroviscous effect in many cases (Hunter, 1981). The primary mechanism of the electroviscous flow is illustrated in Fig. 1b. When an aqueous solution flows through a micro-channel driven only by a pressure difference, the counterions in the diffuse layer are carried toward the outlet end, resulting in the formation of streaming potential along the flow direction. Subsequently, the flow-induced streaming potential drives the counterions to move against the liquid flow direction. Meanwhile, the moving counterions in the diffuse layer will drag the liquid molecules to migrate. The net effect results in an increase in the fluid viscosity and thus the reduction in the flow rate through a micro-channel, i.e., so-called the electroviscosity effect (Wang et al., 2006).

The impact of generated streaming potential on the flow of formation fluids (i.e., electrolyte solutions) through low permeable rocks cannot be arbitrarily neglected (Bear, 2013; Donaldson and Alam, 2013). Zhang et al. (2015) studied the electrokinetic flow of a Newtonian fluid in a capillary tube with periodically varying cross-sections and concluded that the electroviscous effects cannot account for the observed nonlinear flow in tight porous media. Besides, we recently examined the flow characteristics of solutions in hydrophilic nanopores considering the electroviscous effects and the enhanced viscosity near the charged wall, yet the nonlinear fluid flow was not found (Cheng et al., 2020). Additionally, the formation liquids generally carry mineral particles and may become non-Newtonian liquids due to clay-water interactions (Swartzendruber, 1962a; Swartzendruber, 1962b; Liu et al., 2012). Such fluids have also been considered as Bingham fluids in numerical studies (Jiang et al., 2012; Zhang et al., 2019). Published experimental studies also show that clay-water suspensions can behave as non-Newtonian Bingham fluids with yield stress (Rand and Melton, 1977; Torrance, 1999; Amorós et al., 2010). Further, it has been stated that the nonlinear flow is likely to take place in any surface-active porous medium, and the non-Newtonian behavior can be a

possible cause of the non-Darcy flow (Swartzendruber, 1962a,b), which has not yet been validated. Based on the above discussion, we here consider the formation liquids as the Bingham fluids and investigate whether the nonlinear flow found in published experiments can be interpreted by the combined effects of the electrokinetic flow and the non-Newtonian rheology. Recently, based on the Debye-Huckel linearization theory (Kirby, 2010), a closed-form model of the electrokinetic flow of Bingham-plastic fluid (Zhang et al., 2019) has been proposed to account for the nonlinear flow mechanism in circular pores; however, it cannot consider the impacts of high zeta potential at the solid wall due to the linearization simplification.

This study aims to investigate the electroviscous flow in a micro-sized capillary tube using a continuous Bingham-Papanastasiou (BP) fluid (Papanastasiou, 1987). This non-Newtonian fluid model is chosen to avoid the inherent attribute of discontinuity in the ideal Bingham-plastic model (Mitsoulis, 2007). After detailed descriptions of the model and model validation, we investigate the impacts of fluid rheological properties and electrokinetic parameters on the electrokinetic flow characteristics. The results help shed light on the understanding of low-velocity nonlinear flow of formation fluids in tight media.

2. Numerical model

2.1. Governing equations

The fluid viscosity η is a constant for Newtonian fluids, but a shear-dependent variable for non-Newtonian fluids. For the BP fluid, η is defined by (Papanastasiou, 1987)

$$\eta = \frac{\tau}{\dot{\gamma}} = \eta_0 + \frac{\tau_0}{\dot{\gamma}}[1 - \exp(-m\dot{\gamma})] \tag{1}$$

where η_0 is the plastic viscosity; m is the stress growth index that controls the strength of the increasing stress; τ_0 denotes the yield stress, and τ is the shear stress corresponding to a specific shear rate. Additionally, the shear rate tensor γ is expressed as (Bird et al., 1987)

$$\dot{\gamma} = \sqrt{2\mathbf{S}\colon \mathbf{S}} \tag{2}$$

where S is calculated by

$$\mathbf{S} = [\nabla\mathbf{u} + (\nabla\mathbf{u})^T]/2 \tag{3}$$

in which, u is the fluid velocity. Fig. 2 illustrates the rheological behavior of BP fluids with various m values. The results are presented in dimensionless shear stress τ/τ_0 with increasing shear rate $\dot{\gamma}$. An important feature of the BP fluids is that they have a finite stress level at small shear rates, unlike the ideal Bingham model in which a solid-like structure is formed as $\tau < \tau_0$. Furthermore, the Newtonian fluid is recovered when m approaches 0 or $\tau_0 = 0$. In the limit of $m \to \infty$, Eq. (1) is reduced to the classical Bingham-plastic model (Mitsoulis, 2007).

This study considers the steady-state laminar flow of a binary electrolyte, i.e., an incompressible non-Newtonian fluid with viscosity η, flowing through a cylindrical microtube with radius r subjected to a pressure gradient P_z. The flow velocity u can be characterized by the modified Navier-Stokes (N-S) equation:

$$\frac{d^2u}{dr^2} + \frac{1}{r}\frac{du}{dr} = -\frac{P_z}{\eta} - \frac{E_s}{\eta}\rho_e \tag{4}$$

where E_s and ρ_e are induced electric field strength and charge density, respectively.

The electrical potential distribution of the solution in a capillary tube is governed by the Poisson equation (Hunter, 1981):

$$\frac{d^2\psi}{dr^2} + \frac{1}{r}\frac{d\psi}{dr} = -\frac{\rho_e}{\varepsilon_0\varepsilon_r} \tag{5}$$

where ψ is the electrostatic potential; ε_0 is the vacuum permittivity; and ε_r is the relative permittivity of the fluid. The charge density ρ_e can be determined by

$$\rho_e = \sum_i e z_i n_i \tag{6}$$

where e is the elementary charge; z_i and n_i denote the valence and the number concentration of the ith species. When the advection of ions is neglected, by combining the assumption of electro-neutrality far away from the walls, n_i can be given by

$$n_i = n_{i,\infty}\exp\left(-\frac{z_i e\psi}{k_B T}\right) \tag{7}$$

where $n_{i,\infty}$ is the bulk ionic concentration of the ith species; k_B is the Boltzmann constant; and T is the environment temperature. Summarizing Eqs. (5)–(7) then leads to the Poisson Boltzmann (PB) equation

$$\frac{d^2\psi}{dr^2} + \frac{1}{r}\frac{d\psi}{dr} = \frac{2n_\infty ze}{\varepsilon_0\varepsilon_r}\sinh\left(\frac{ze\psi}{k_B T}\right) \tag{8}$$

Note that E_s in Eq. (4) is determined with the net electrical current being zero in the steady-state, which means

$$I = I_c + I_s = 0 \tag{9}$$

where I, I_c, and I_s are the net electrical current, the conduction current, and the streaming potential, respectively. Hence, E_s can be given by (Rice and Whitehead, 1965)

$$E_s = -\frac{2\pi\int_0^R \rho_e u(r) r dr}{\lambda_{eff} A_c} \tag{10}$$

where R is the capillary tube radius; A_c is the cross-sectional area of the microtube; and λ_{eff} is the effective electric conductivity of the liquid that can be analytically determined by (Ban et al., 2010)

$$\lambda_{eff} = \frac{2\pi\int_0^R \lambda r dr}{A_c} \tag{11}$$

where the electric conductivity λ can be expressed as (Lu et al., 2004; Ban et al., 2010)

$$\lambda = \sum \frac{z_i^2 e^2 D_i n_i}{k_B T} \tag{12}$$

where D_i is the diffusion constant of the ith species. As such, the distributions of electrical potential and charge density can be calculated using the PB model, and the velocity profile in a microtube is obtained through the modified N-S equation Eq. (4).

2.2. The numerical model and model validation

To reduce the computational cost of solving the PB and the modified N-S equations, a two-dimensional axisymmetric model is used in the simulations. The model (Fig. 3) shows a capillary tube with a radius R, a solid wall (BC boundary) with zeta potential ζ, and a pressure difference between the inlet P_{in} (AB boundary) and outlet P_{out} (CD boundary) of the capillary tube. No-slip boundary condition ($u = 0$) is assumed at the solid wall (BC boundary). Given that the coupled model incorporating the PB and the modified N-S equations are highly

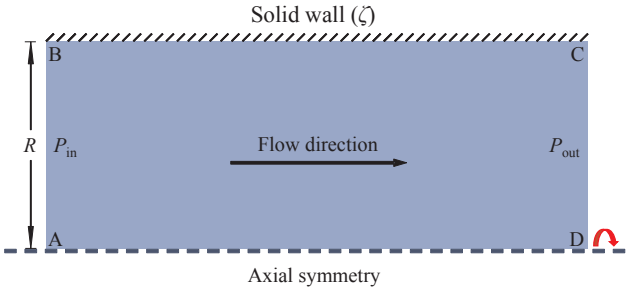

Fig. 3. The 3D cylindrical model is simplified to the 2D axisymmetric model.

nonlinear, the COMSOL package (based on the finite element method) is employed to numerically solve these equations (Multiphysics, 2012).

Since no analytical solution to the electrokinetic transport of the BP fluid in a capillary tube exists, the validation of the numerical model in this study is confirmed by simulating the electrokinetic flow of a Newtonian fluid (a 1:1 electrolyte solution) in a capillary tube and comparing to its approximate analytical solution.

Regarding Eq. (8), the term $\sinh(ze\psi/k_BT)$ can be approximately written as $(ze\psi/k_BT)$ when the zeta potential of the charged wall is low ($|ze\psi/k_BT| \leqslant 1$), namely the Debye-Huckel approximation (Kirby, 2010). Hence, the PB equation is linearized as

$$\frac{d^2\psi}{dr^2} + \frac{1}{r}\frac{d\psi}{dr} = \frac{2n_\infty z^2e^2}{\varepsilon_0\varepsilon_r k_BT}\psi = \kappa^2\psi \tag{13}$$

where $\kappa = \sqrt{2n_\infty z^2e^2/(\varepsilon_0\varepsilon_r k_BT)}$ represents the reciprocal of the Debye length, which is the nominal thickness of the EDL. As such, κR, the ratio of the microtube radius over the EDL thickness, indicates the relative intensity of the electrokinetic effects. Combing Eq. (5) and (13), the EDL electrical potential and the velocity profile within the microtube can be analytically determined (Rice and Whitehead, 1965),

$$\psi(r) = \zeta\frac{I_0(\kappa r)}{I_0(\kappa R)} \tag{14}$$

$$u(r) = \frac{1}{4\eta}P_z(R^2 - r^2) - \frac{\Omega^2 P_z\left[1 - \frac{I_0(\kappa r)}{I_0(\kappa R)}\right]}{\lambda_s}\frac{1 - \frac{2I_1(\kappa R)}{\kappa R I_0(\kappa R)}}{1 - \beta\left[1 - \frac{2I_1(\kappa R)}{\kappa R I_0(\kappa R)} - \frac{I_1^2(\kappa R)}{I_0^2(\kappa R)}\right]}, \tag{15}$$

where I_0 and I_1 are the zero-order and first-order modified Bessel function, respectively. Besides, two coefficients are expressed as: $\Omega = \varepsilon\psi_0/\eta$ and $\beta = \Omega^2\eta\kappa^2/\lambda_s$.

The following parameter values are assumed for the comparison of analytical and numerical results. The electric conductivity λ is taken as a constant 8×10^{-8} S/m, and the ionic molar concentration c_∞ is 10^{-6} mol/L. Note that the correlation between n_∞ and c_∞ is $n_\infty = c_\infty \times N_A$, where N_A is the Avogadro constant. The density, viscosity, and relative permittivity of the solution are taken as 1000 kg/m^3, 1 mPa·s, and 80, respectively. The temperature is 298.15 K, and the pressure gradient imposed is 1 MPa/m.

Fig. 4 shows the distribution of electrical potential and the velocity profile using the simulation and the analytical solution. The numerical results perfectly agree with that of the Debye-Huckel theory when $\zeta = -20$ mV (Fig. 4a). However, as expected, the numerical PB solution gradually departs from the Debye-Huckel prediction when $\zeta = -60$ and -100 mV, because the Debye-Huckel approximation is only valid under low ζ. As for the velocity profiles (Fig. 4b), numerical results are lower than that from the Hagen-Poiseuille (HP) velocity for all ζ values, highlighting the electroviscous effect on retarding the fluid flow in microtubes. At $\zeta = -20$ mV, the velocity profile by the PB model is in good agreement with that of the Debye-Huckel method. However, the differences between the analytical and the simulation results increase with increasing ζ values, and the Debye-Huckel approach underestimates the fluid velocity. Thus, the numerical solution of the coupled PB and modified N-S equations can not only provide validated results but also capture the electroviscous effect particularly at high zeta potential of the solid wall.

3. Numerical results

The transport characteristics of the BP fluid through a microtube are investigated considering the surface zeta potential ζ, the ionic molar concentration c_∞, the fluid stress growth index m, and the fluid yield stress τ_0. The characteristics of the Newtonian fluid flowing through the microtube are also presented as a comparison. The following simulations assume a potassium chloride (KCl) solution, which is a common component of the formation fluid in tight reservoirs. All other parameters used in the simulations including temperature, the pressure gradient, and viscosities are listed in Table 1. Note that the plastic viscosity also represents the viscosity of the Newtonian liquid.

3.1. Induced electrical potential

The manifested electroviscous effect on fluid flow through a microtube is caused by the movement of counterions within the EDL against the pressure gradient. The induced electrokinetic resistance is largely associated with the strength of the generated streaming potential. Thus, we here consider the influence of the yield stress τ_0 on the induced electrical field strength $|E_s|$.

A BP fluid can be reduced to the Newtonian fluid when the yield stress $\tau_0 = 0$ (see Eq. (1)). As such, both Newtonian and non-Newtonian fluids show an identical electrical strength when fluid yield stress $\tau_0 = 0$ (Fig. 5). The Newtonian fluid always holds a constant electrical strength $|E_s|$ and is larger than that of the BP fluid, regardless of the changing yield stress. This is because the BP fluid has a higher viscosity than the Newtonian fluid, causing a reduction in the flow velocity, the mobility of the electrical charge, and thus the induced electrical field strength. In other words, the BP fluid can lower the streaming potential (Zhang et al., 2019). Additionally, as the fluid yield stress τ_0 increases,

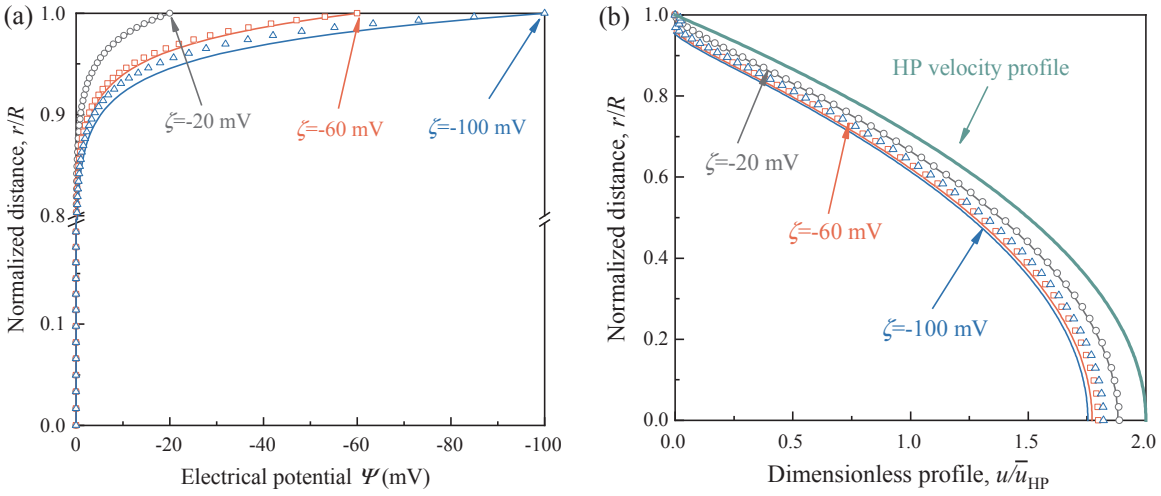

Fig. 4. Comparisons of the results from the Debye-Huckel linear method (solid lines) and the PB equation (open markers) when $\kappa R = 30$. (a) The electrical potential distribution; (b) The dimensionless velocity distribution, where $\bar{u}_{HP}$ represents the HP average velocity of the fluid without involving the electroviscous effects.

Table 1
The main parameters used for simulation.

Parameter description	Symbol	Unit	Value
Temperature	T	K	298.15
Relative permittivity	ε_r	–	80
Molar concentration	c_∞	mol/L	10^{-7}
Valence of K^+	z_1	–	1
Valence of Cl^-	z_2	–	−1
Diffusion coefficient of K^+	D_1	m^2/s	1.957×10^{-9} (Haynes, 2014)
Diffusion coefficient of Cl^-	D_2	m^2/s	2.032×10^{-9} (Haynes, 2014)
Plastic viscosity	η_0	mPa·s	1
Viscosity of the Newtonian fluid	η_0	mPa·s	1
Pressure gradient	–	MPa/m	1

the flow velocity also decreases due to increased viscous resistance and thus the induced electrical field $|E_s|$ as shown in Fig. 5. As shown in Fig. 5c and 5d, the induced electrical field $|E_s|$ in a microtube with radius $R = 10\,\mu m$ does not show an evident difference as the fluid stress growth index m varies from 0.1 to 1000 s. This is mainly because the shear stress of the BP fluid is less dependent on a certain range of shear rate (see also Fig. 2) so that the difference in viscosity becomes negligible when $m > 0.1$ s.

The induced electrical field $|E_s|$ generally decreases and departs from that of the Newtonian fluid as the m value increases. The decreasing trend in $|E_s|$ with increasing m values is also affected by the fluid yield stress τ_0 particularly when $m > 0.1$ s. This phenomenon is more pronounced in smaller microtubes, such as in a 3-μm radius microtube shown in Fig. 5a and 5c. When the fluid yield stress is high, say $\tau_0 > 1.4$ Pa, the flow velocity is relatively low, resulting in a weak electrical field $|E_s|$. While in a $R = 10\,\mu m$ microtube, the induced electrical field is still relatively high compared to that in the $R = 3\,\mu m$ microtube at a high fluid yield stress $\tau_0 = 2$ Pa. This is attributed to the higher fluid velocity within the $R = 10\,\mu m$ microtube. Furthermore, it is also found that although a larger zeta potential corresponds to a larger net charge density, the induced $|E_s|$ in this scenario is lower. This finding is similar to the study of Jamaati et al. (2010), in which, a decrease in $|E_s|$ with increasing zeta potential is observed when the zeta potential is higher than a critical value. This reflects that the electric field $|E_s|$ is determined by multiple factors according to Eq. (10) and higher charge density ρ_e may be counteracted by higher electrical conductivity λ_{eff} of the liquid.

3.2. Velocity profiles

Fig. 6 presents the velocity profiles of non-Newtonian fluids through microtubes with the consideration of the electrokinetic effect. The velocity results are presented in a dimensionless form, i.e., divided by the average bulk velocity $\bar{u}_{hp}$. Note also that the results for the cases of

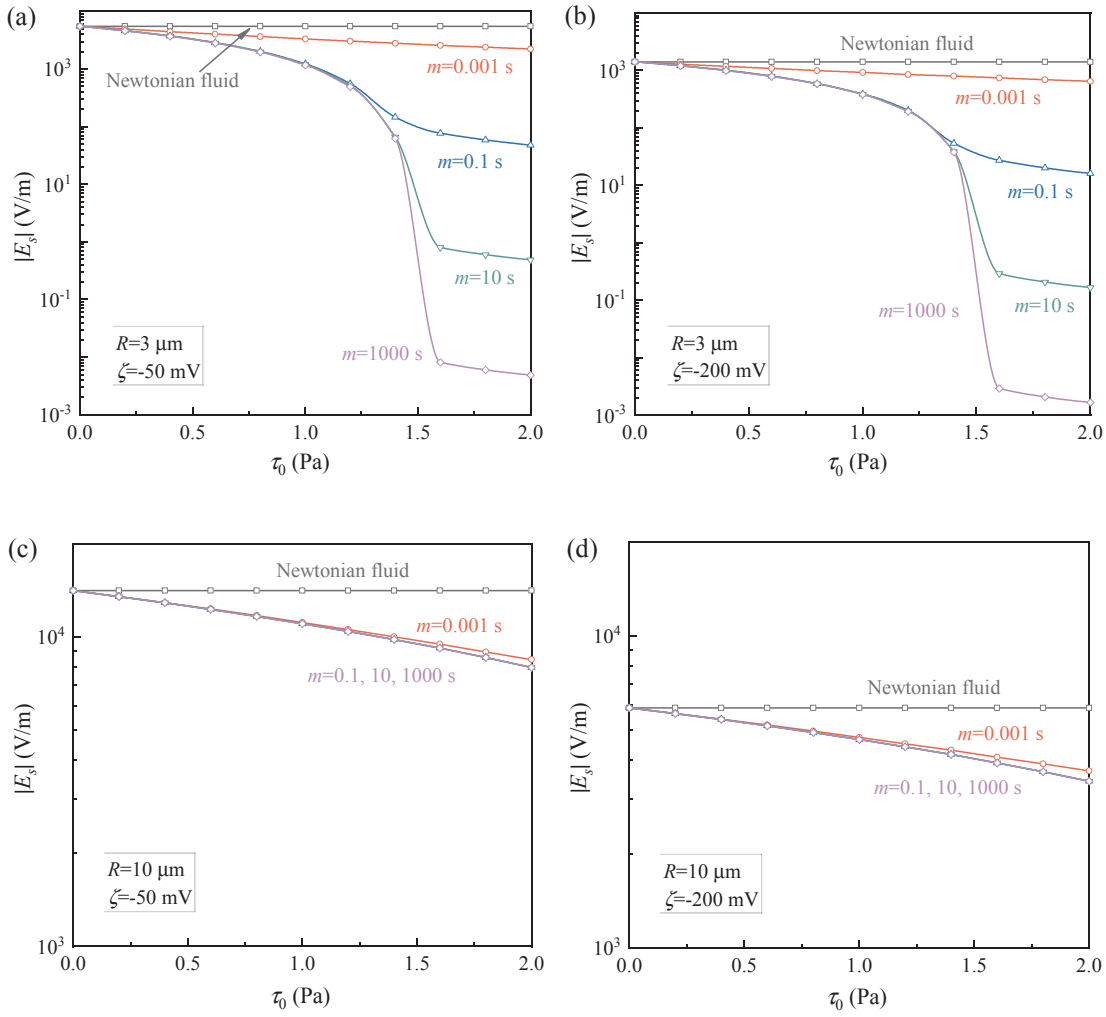

Fig. 5. Dependence of $|E_s|$ on the yield stress τ_0 for various values of m, zeta potential ζ, and capillary radius R. Note that for (c) and (d), results of $m = 0.1$ s and $m = 10$ s are nearly overlapping with that of $m = 1000$ s.

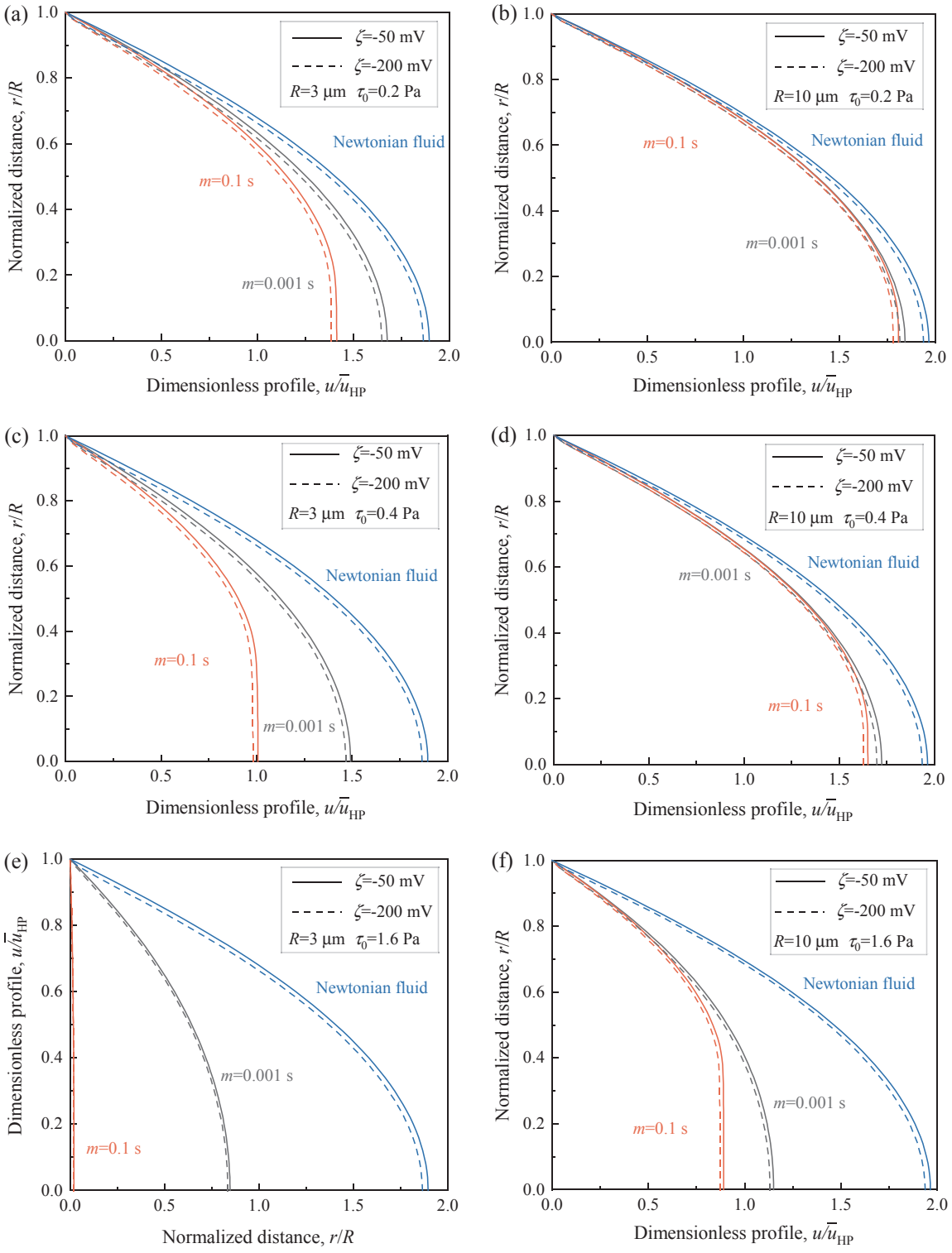

Fig. 6. Dimensionless velocity (u/ ūHP) profiles across the microtube at various values of m, R, ζ and τ_0, where the velocity distributions of the Newtonian fluids are plotted for comparison as well.

m = 10 s and 1000 s are not shown as they almost overlap with that of the m = 0.1 s case, as discussed previously in Section 3.1.

The results show that the Newtonian fluid has higher velocities at all radial positions within the capillary tube than that of the non-Newtonian fluids, even though the Newtonian fluid has higher electrokinetic resistance (as shown in Fig. 5). This is mainly due to the high viscosity of the BP fluids that outweighs the electroviscous effects. Additionally, as the zeta potential of the wall shifts from −50 mV to −200 mV, there is a slight decrease in the velocity due to increased electrokinetic resistance. As such, the shear rate of the fluid decreases when the yield stress increases, particularly near the central region of the capillary tube. This leads to flatter velocity profiles of the non-Newtonian fluids, i.e., no longer parabola profiles (Fig. 6c). Such velocity profiles can also be found in the published numerical study (Tang et al., 2011). The calculated velocity profiles in the 10-μm microtubes (Fig. 6b, 6d, and 6f) follow a similar pattern as those of the 3-μm

microtubes (Fig. 6a, 6c, and 6e). However, the latter has more pronounced electroviscous effects and Bingham behaviors of fluids. The more pronounced electroviscous effect in the 3-μm microtubes is attributed to the thicker EDL compared to that in the 10-μm microtubes.

Furthermore, the velocity declines more rapidly as the yield stress increases in the 3-μm microtube compared to the 10-μm microtube. For instance, the maximum dimensionless velocity is only 0.02 when τ_0 = 1.6 Pa and m = 0.1 s in the 3-μm microtube, indicating enormous flow resistance resulted from the Bingham rheology. This result further supports the above observation that very low fluid velocity cannot lead to significant streaming potential (Fig. 5a and b).

4. Analyses and discussion

4.1. Apparent viscosity

The apparent viscosity of the fluid flow in the microtubes η_{app} is calculated to quantitatively evaluate the strength of the flow resistance induced by the electrokinetic effect. The results are presented in dimensionless η_{app}/η^*, i.e., divided by the viscosity of the non-Newtonian fluid η^*. Note that at a constant pressure gradient, η_{app}/η^* essentially reflects $u_{non\text{-}eve}/u_{eve}$, where $u_{non\text{-}eve}$ and u_{eve} are the averaged flow velocity in a microtube without and with the consideration of the electroviscous forces, respectively. Note that the averaged flow velocity also inherently captures the flux in the microtube.

Fig. 7a depicts the effects of the capillary radius on η_{app}/η^* for both the Newtonian and the BP liquids with different m values. For non-Newtonian fluids, η_{app}/η^* is used for reflecting the effect of streaming potential on fluid flow; hence, it is always larger than unity. The results show that η_{app}/η^* varies non-monotonically with the microtube size. For instance, with the increase in the tube size, η_{app}/η^* first experiences a rapid increase, followed by a gradual decrease when m = 0.1 s. Overall, the electrokinetic effect in the non-Newtonian fluid is sensitive to the value of m, and the resulted viscosity can be higher or lower than that of the Newtonian fluid. The total flow resistance in a microtube is mainly caused by the viscous drag and the electroviscous force within the EDL. Subjected to a certain pressure gradient, the fluid with m = 0.01 s or 0.1 s has a relatively low shear rate in a small-sized microtube (e.g., R < 3 μm) that leads to a high viscosity in the microtube. In these situations, the flow resistance is dominated by the viscous forces, leading to a lower η_{app}/η^* value. With the increase in the microtube size, the electroviscous contribution to the flow resistance will be enhanced due to increased flow shear rate, followed by a gradual decrease due to reduced EDL thickness compared to the tube size, and eventually approaches to one (as shown in Fig. 7a). Plus, the difference in η_{app}/η^* among different m values diminishes as R > 15 μm. This result may be because the viscosity of the non-Newtonian fluid is independent of the m value under a certain range of shear rates (refer to Fig. 2). Therefore, it can be concluded that the variation in η_{app}/η^* with the values of microtube radius and m is not monotonous, and η_{app}/η^* has a local maximum at a certain capillary radius, which is strongly related to the rheological properties of the fluids.

Furthermore, the relationship between η_{app}/η^* and the yield stress of the fluid is presented in Fig. 7b. The Newtonian liquid has a constant

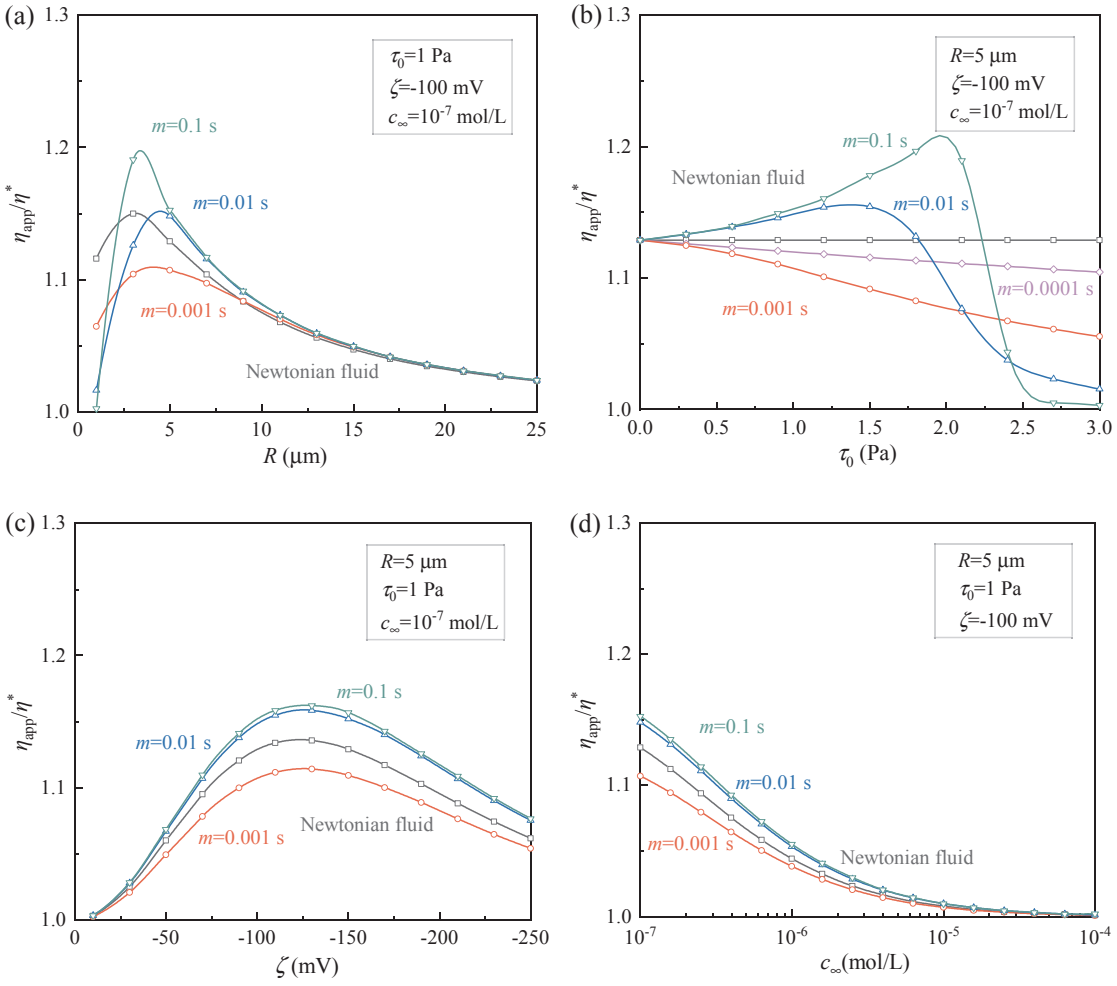

Fig. 7. The variation of dimensionless apparent viscosity as a function of (a) capillary radius R, (b) yield stress τ_0, (c) zeta potential ζ, and (d) molar concentration of the solution c_∞.

η_{app}/η^* regardless of τ_0 as expected. When $m = 0.001$ s, the dimensionless apparent viscosity η_{app}/η^* of the liquid decreases almost linearly and would be close to unity with the yield stress, and the difference in η_{app}/η^* between the non-Newtonian and the Newtonian fluids becomes larger as τ_0 increases. Likewise, reducing the m value would reduce the difference in η_{app}/η^* between the two fluids (see the case of $m = 0.0001$ s in Fig. 7b). However, the effect of τ_0 on the η_{app}/η^* of non-Newtonian fluids is non-monotonic when $m > 0.001$ s, and there exists a critical τ_0 that resulting in the largest η_{app}/η^*. It is also revealed that the m value has a non-monotonic influence on η_{app}/η^*. The η_{app}/η^* versus τ_0 trends are different at different m values. This is mainly because the increase in η^* outweighs the electrokinetic resistance at small m values (i.e., $m = 0.0001$ and 0.00001 s herein), and a greater electrokinetic contribution to the increases fluid viscosity at larger m values (i.e., $m = 0.01$ and 0.1 s). However, the very low flow rate will make the electroviscous effect negligible at a larger τ_0. Specifically, at $m = 0.1$ s and $\tau_0 > 2.7$ Pa, the electroviscous effect becomes subtle mainly due to the very low shear rate in the flow. The viscous and electroviscous forces accounting for the proportions of the total flow resistance changes as τ_0 increases, and the magnitude of the electrokinetic effects is notably dependent on the fluid rheology.

Fig. 7c shows the impact of zeta potential ζ on the electroviscous flow of Newtonian and non-Newtonian fluids. The apparent viscosity of the Newtonian fluid η_{app}/η^* exhibits a non-monotonic behavior with increasing ζ. This result is qualitatively consistent with previous studies (Jamaati et al., 2010; Jing et al., 2017). The most remarkable electroviscous effect occurs when $m = 0.01$ s. Additionally, the dependence of η_{app}/η^* on the zeta potential for three cases of non-Newtonian fluids is also non-monotonic. Also, η_{app}/η^* varies non-monotonically with the m value in some instances (Fig. 7a).

The role of the solution concentration c_∞ in fluid transport in microtubes is investigated. As illustrated in Fig. 7d, a higher m value results in a larger η_{app}/η^*. In addition, the η_{app}/η^* monotonically decreases with increasing ionic molar concentration c_∞, which reduces the EDL thickness and thus the electroviscous resistance of fluids. There are numerical studies (Masliyah and Bhattacharjee, 2006; Wang et al., 2006) showing the non-monotonic dependence of η_{app}/η^* on the solution concentration, while Bharti et al. (2008) and Bharti et al. (2009) did not observe a local maximum of η_{app}/η^*, as presented in this study. This inconsistency is likely related to the differences in the boundary conditions (i.e., a constant ζ versus a constant surface charge density) or the calculation of the electrical conductivity of the solution. In the work of Wang et al. (2006), λ_{eff} was set as a constant. However, as for the electroviscous flow, the electric conductivity of an electrolyte is a key parameter to determine the streaming potential. It is a function of the ion type, ion concentration, and zeta potential; thus, using a fixed λ_{eff} in the simulation may not be appropriate. Here, following Ban et al. (2010), λ_{eff} is determined by using Eq. (12), which captures the influences of these factors and is also in line with the calculation method of λ_{eff} adopted in Bharti et al. (2008) and Bharti et al. (2009).

4.2. Nonlinear flow characteristics

Fig. 8 shows the fluid velocity versus pressure gradient relationship $\bar{u}$-P_z under various influencing factors. The results exhibit the nonlinear characteristics of the flow in microtubes that are successfully captured by considering the BP non-Newtonian fluid and the electrokinetic effect. Fig. 8a and b show that the $\bar{u}$-P_z curves nearly coincided, indicating the marginal effects of the zeta potential ζ and the ionic molar concentration c_∞, particularly when the pressure gradient is low. The difference in the $\bar{u}$-P_z relation becomes more notable at higher pressure gradients. The total flow resistance is dominated by the viscous force at low pressure gradients, and by the electroviscous force at high pressure gradients. This implies that the electrokinetic parameters (ζ, c_∞) have more evident impacts on the electroviscous flow in microtubes at a relatively high-pressure gradient. As shown in Fig. 8c and d, the rheological parameters (m, τ_0) have more pronounced impacts on the nonlinearity of the fluid flow, i.e., more concaved $\bar{u}$-P_z curves. At $m = 0.01$ and 0.1 s, the fluid velocity at a pressure gradient smaller than ~0.5 MPa/m is very low as if there exists a threshold pressure gradient (Fig. 8c). Such flow rates are too low to be accurately measured in a conventional laboratory setting. While at $m = 0.001$ s, the nonlinear behavior is not remarkable. Furthermore, all the $\bar{u}$-P_z relations will collapse into a single trend for various m values at high pressure gradients since the role of the m value in determining the fluid rheology becomes insignificant. In this situation, three curves are nearly parallel to each other. Also, it is again found that for Newtonian fluids, considering the electroviscous effects alone cannot result in the nonlinearity in the $\bar{u}$-P_z relation. Moreover, a larger yield stress τ_0 of the fluid leads to a stronger nonlinearity of flow and a lower flow rate (Fig. 8d). Therefore, the results highlight the dominant role of the electrokinetic parameters (ζ, c_∞) at high pressure gradients and the fluid rheological parameters (m, τ_0) at low pressure gradients on the flow in microtubes.

4.3. Extension to natural tight formations

Unconventional resources such as shale gas and tight oil are always stored in ultra-low permeable reservoirs with abundant nano- to micropores. To understand the unique seepage mechanisms in low permeable reservoirs, laboratory tests generally focus on the single-phase flow through rock samples, as described in the Introduction. Admittedly, using the KCl solution representing the formation fluids is a simplification in this study, as the formation fluids usually involve oil, water and/or gases and the compositions of the formation water are complex. However, given that formation liquids commonly have certain salt concentrations, the resulted electroviscous effects on fluid flow need to be seriously considered. Keep in mind that the EDL does not overlap in all microscale flow simulations in this investigation, and thus, the PB model is still adequate to characterize the distributions of ions and electrical potential.

Furthermore, as described in the Introduction, the fluid rheology may have been altered to be non-Newtonian fluid with yield stress due to charged particles, and the complex interaction between liquid and the mineral surface. A recent analytical study investigated the electroviscous flow of a Bingham-plastic fluid in microsized circular tubes (Zhang et al., 2019), in which the fluid flow occurs only after exceeding the TPG and followed by a linear flow. They also stated that such a generated nonlinear flow behavior coincided with the experimental results for deionized water flowing in silica microtubes (Yang et al., 2011; Zhu et al., 2014). In fact, whether the TPG exists is controversial. According to the viewpoint in the literature (Wang and Sheng, 2017), TPG is generally obtained by fitting the measured $\bar{u}$-P_z curve. And the hydrocarbon migration during the reservoir forming process cannot happen if there is a TPG. The utilization of the BP model in our study generates a continuously nonlinear flow in microtubes without involving the conception of TPG. Moreover, the results in this article indicate that the electroviscous flow of the Newtonian fluid in microtubes shows the linear feature, implying that experiments of deionized water flow in microtubes are probably not ideal for unraveling the mechanism of nonlinear flow in porous materials. The possible reason is that the surface characteristic of microtubes used in testing cannot represent that of reservoir minerals.

The gained new insights can have potential applications for practical reservoir engineering. For instance, the fluids used for permeability measurement in rock samples can be collected for further rheology tests. The viscosity-shear rate results can be fitted by the BP model to acquire rheological parameters for reservoir simulators. In terms of the electrokinetic effect, its significance can be evaluated by the ratio of the EDL thickness over the characteristic length of the porous rock or soil, which is associated with its permeability. The dimensionless apparent viscosity determined in Section 4.1 shows that

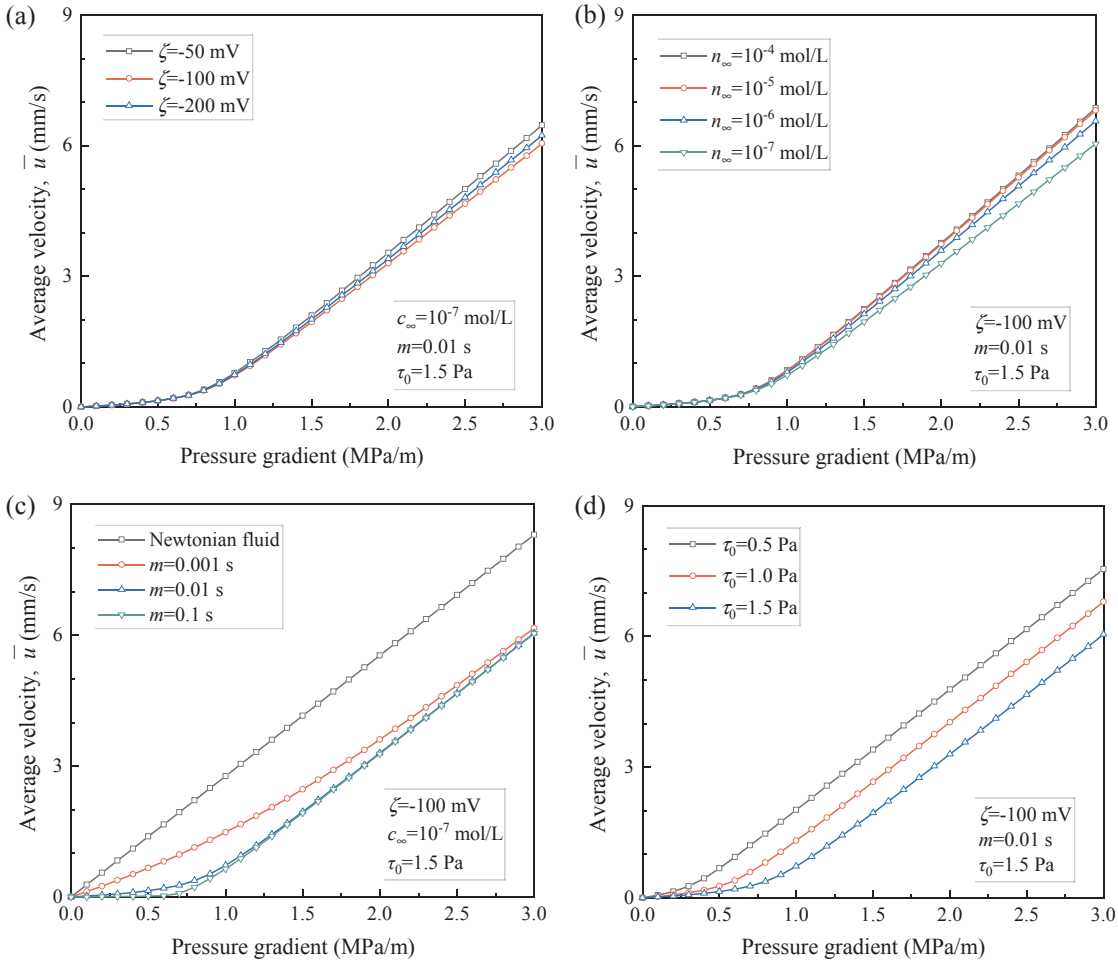

Fig. 8. Average velocity versus pressure gradient for a 5-μm microtube under the effects of various influencing factors: (a) zeta potential ζ, (b) ionic concentration c_∞, (c) stress growth index m, and (d) yield stress τ_0.

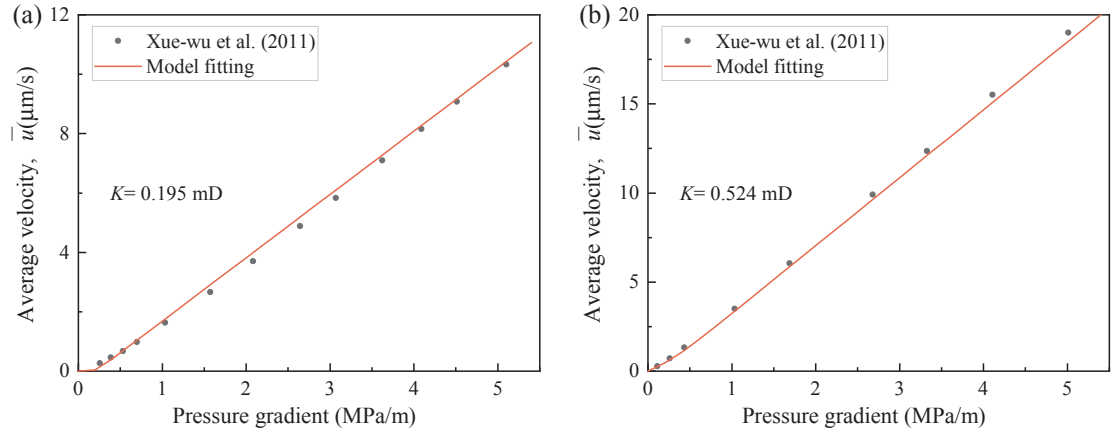

Fig. 9. Comparison of the results from the experiments and the non-Newtonian model estimation, where two low-permeability samples (a) K = 0.195 mD and (b) K = 0.524 mD were equivalent to be the capillary bundle model.

Table 2
Experimental and fitting parameters.

Liquid type	Permeability (mD)	Porosity	R_{eq} (μm)	m (s)	τ_0 (Pa)	η_0 (mPa·s)	ξ (mV)	c_∞ (mol/L)
Formation Water (Xue-wu et al., 2011)	0.195	9.63%	0.128	0.1	10	1	−50	10^{-5}
Formation Water (Xue-wu et al., 2011)	0.524	13.75%	0.175	0.1	0.01	1	−50	10^{-5}

R_{eq} means the equivalent radius of the capillary bundle.

the electroviscous effect is not quite notable in micropores, but it could become potentially more significant electroviscous effect in nanopores. In this case, a more general Poisson–Nernst–Planck model may be required to characterize the electrokinetic transport because of the overlapped EDL (Zhang and Wang, 2015). Additionally, the slip boundary condition should also be considered (Jing et al., 2017; Hajmohammadi et al., 2018), which depends on the solid-liquid interaction and is out of our subject here.

Using the micro-flux measuring instrument, Xue-wu et al. (2011) acquired the apparent permeability of sandstone cores under different pressure gradients and observed the low-velocity non-Darcy behavior. Based on the assumption that the core can be simplified by the capillary bundle model (Bear, 2013), we replot the velocity-gradient curves of two samples, shown in Fig. 9. The curves are fitted using the non-Newtonian model adopted in this work. All relevant experimental and fitting parameters are listed in Table 2. The fitting results are in good accord with the experimental data, indicating the nonlinear flow can be generated through the combination of non-Newtonian rheology and electroviscous effect, which may be a possible mechanism responsible for the low-velocity non-Darcy flow of fluids in low permeable formations.

In sum, the insights gained from this paper can enhance current reservoir simulators and provide theoretical foundations to broader fields, such as the design of microfluidic devices, soil, hydrology engineering, and geophysical applications.

5. Conclusions

In this study, the electrokinetic transport of BP non-Newtonian fluids through circular microtubes was systematically studied using the coupled PB and N-S equations. The effects of various electrokinetic and rheological properties on the induced electrical field strength, velocity profile, and transport capacity of the non-Newtonian fluid flow in microtubes were examined. Furthermore, the characteristics of the nonlinear flow of fluids in microchanels were analyzed as well. The main conclusions are drawn as follows:

(1) The induced electrical strength $|E_s|$ is collectively determined by various parameters, such as the fluid velocity, the electric conductivity, and charge density within EDL. Under the same condition, $|E_s|$ for the non-Newtonian fluid is lower since it has a higher viscosity than the Newtonian liquid. In addition, $|E_s|$ will monotonously decrease as τ_0 increases, and can almost be ignored especially for the microtube with a small radius. Besides, due to the fluid rheology of the BP model, $|E_s|$ is not sensitive to the variation of m when $m > 0.1$ s, while decreasing m would enable $|E_s|$ to be closer to that for the Newtonian fluid when $m < 0.1$ s. As such, at a fixed pressure gradient, a larger capillary will result in a higher $|E_s|$.

(2) The velocity profiles of non-Newtonian fluids will become lower and flatter when τ_0 or m increases and a region having a higher viscosity would occur near the microtube center. This phenomenon is more pronounced for the small capillary. In addition, the influences of the capillary size R, zeta potential ζ, stress growth index m, and yield stress τ_0 on η_{app}/η^* for both of the Newtonian and BP fluids are not monotonous, and there is a critical value that leads to the largest η_{app}/η^* for each case; while η_{app}/η^* gradually decreases with the increasing ion concentration c_∞ due to the thinner EDL.

(3) With consideration of the non-Newtonian fluid rheology and electroviscous effects, the low-velocity nonlinear flow in microtubes is successfully captured. The electrokinetic parameters (ζ, c_∞) only affect the flow characteristic of fluids at the high-pressure gradient but have negligible effects on the fluid flow when the pressure gradient is relatively low. In contrast, the rheological parameters (m, τ_0) highly control the magnitude of the flow nonlinearity, in particular at the low-pressure gradient. Additionally, only considering the electroviscous effects of the Newtonian fluid cannot produce the nonlinear regime.

CRediT authorship contribution statement

Zhilin Cheng: Conceptualization, Methodology, Software, Writing - original draft. **Zhengfu Ning:** Supervision, Resources. **Sheng Dai:** Supervision, Investigation, Writing - review & editing.

Declaration of Competing Interest

The authors declare that they have no known competing financial interests or personal relationships that could have appeared to influence the work reported in this paper.

Acknowledgements

The authors would like to acknowledge the support of the National Natural Science Foundation of China (Grant No. 51504265, 51474222, 51774298 and 51974330), PetroChina Innovation Foundation (2017D-5007-0205) , the China Scholarship Council, and the U.S. National Science Foundation (CMMI-1943722). Any opinions, findings and conclusions expressed in this material are those of the authors and do not necessarily reflect those of the funding agencies. The authors also like to thank the anonymous reviwers for their comments that have significantly improved this manuscript.

Appendix A. Supplementary data

Supplementary data to this article can be found online at https://doi.org/10.1016/j.jhydrol.2020.125224.

References

Amorós, J.L., Beltrán, V., Sanz, V., Jarque, J.C., 2010. Electrokinetic and rheological properties of highly concentrated kaolin dispersions: Influence of particle volume fraction and dispersant concentration. Appl. Clay Sci. 49 (1–2), 33–43.
Ayoubloo, K.A., Ghalambaz, M., Armaghani, T., Noghrehabadi, A., Chamkha, A.J., 2019. Pseudoplastic natural convection flow and heat transfer in a cylindrical vertical cavity partially filled with a porous layer. Int. J. Numer. Meth. Heat Fluid Flow.
Ban, H., Lin, B., Song, Z., 2010. Effect of electrical double layer on electric conductivity and pressure drop in a pressure-driven microchannel flow. Biomicrofluidics 4 (1), 014104.
Bear, J., 2013. Dynamics of Fluids in Porous Media. Courier Corporation.
Bharti, R.P., Harvie, D.J., Davidson, M.R., 2008. Steady flow of ionic liquid through a cylindrical microfluidic contraction–expansion pipe: electroviscous effects and pressure drop. Chem. Eng. Sci. 63 (14), 3593–3604.
Bharti, R.P., Harvie, D.J., Davidson, M.R., 2009. Electroviscous effects in steady fully developed flow of a power-law liquid through a cylindrical microchannel. Int. J. Heat Fluid Flow 30 (4), 804–811.
Bird, R.B., Armstrong, R.C., Hassager, O., 1987. Dynamics of polymeric liquids, vol. 1: Fluid mechanics.
Brutin, D., Tadrist, L., 2003. Experimental friction factor of a liquid flow in microtubes. Phys. Fluids 15 (3), 653–661.
Chen, Z., Liao, X., Zhao, X., Lyu, S., Zhu, L., 2017. A comprehensive productivity equation for multiple fractured vertical wells with non-linear effects under steady-state flow. J. Petrol Sci. Eng. 149, 9–24.
Cheng, Z., Ning, Z., Yu, X., Wang, Q., Zhang, W., 2019. New insights into spontaneous imbibition in tight oil sandstones with NMR. J. Petrol Sci. Eng. 179, 455–464. https://doi.org/10.1016/j.petrol.2019.04.084.
Cheng, Z., Ning, Z., Zhang, W., Ke, S., 2020. Theoretical investigation of electroviscous flows in hydrophilic slit nanopores: Effects of ion concentration and pore size. Phys. Fluids 32 (2), 022005.
Coles, M.E., Hartman, K.J., 1998. Non-Darcy Measurements in Dry Core and the Effect of Immobile Liquid, SPE Gas Technology Symposium. Society of Petroleum Engineers, Calgary, Alberta, Canada, pp. 10. DOI:10.2118/39977-MS.
Dejam, M., Hassanzadeh, H., Chen, Z., 2017. Pre-darcy flow in porous media. Water Resour. Res. 53 (10), 8187–8210.
Diwu, P., Liu, T., You, Z., Jiang, B., Zhou, J., 2018. Effect of low velocity non-Darcy flow on pressure response in shale and tight oil reservoirs. Fuel 216, 398–406.
Donaldson, E.C., Alam, W., 2013. Wettability. Elsevier.
Ghalambaz, M., Chamkha, A.J., Wen, D., 2019. Natural convective flow and heat transfer of nano-encapsulated phase change materials (NEPCMs) in a cavity. Int. J. Heat Mass Transfer 138, 738–749.
Hajmohammadi, M., Alipour, P., Parsa, H., 2018. Microfluidic effects on the heat transfer enhancement and optimal design of microchannels heat sinks. Int. J. Heat Mass

Transfer 126, 808–815.
Hao, F., et al., 2008. Threshold pressure gradient in ultra-low permeability reservoirs. Pet. Sci. Technol. 26 (9), 1024–1035.
Haynes, W.M., 2014. CRC handbook of chemistry and physics. CRC Press.
Huang, Y., Yang, Z., He, Y., Wang, X., Luo, Y., 2013. Nonlinear porous flow in low permeability porous media. Mech. Eng 35 (5), 1–8.
Hunter, R.J., 1981. Zeta potential in colloid science: principles and applications. Academic press, pp. 2.
Jamaati, J., Niazmand, H., Renksizbulut, M., 2010. Pressure-driven electrokinetic slip-flow in planar microchannels. Int. J. Therm. Sci. 49 (7), 1165–1174.
Jiang, R., Li, L., Xu, J., Yang, R., Zhuang, Y., 2012. A nonlinear mathematical model for low-permeability reservoirs and well-testing analysis. Acta Pet. Sin 33 (2), 264–268.
Jing, D., Pan, Y., Wang, X., 2017. The non-monotonic overlapping EDL-induced electroviscous effect with surface charge-dependent slip and its size dependence. Int. J. Heat Mass Transfer 113, 32–39.
Kirby, B.J., 2010. Micro-and nanoscale fluid mechanics: transport in microfluidic devices. Cambridge University Press.
Kumar, K.G., Rahimi-Gorji, M., Reddy, M.G., Chamkha, A.J., Alarifi, I.M., 2020. Enhancement of heat transfer in a convergent/divergent channel by using carbon nanotubes in the presence of a Darcy-Forchheimer medium. Microsyst. Technol. 26 (2), 323–332.
Li, D., 2004. Electrokinetics in microfluidics. Elsevier.
Liu, H.-H., Li, L., Birkholzer, J., 2012. Unsaturated properties for non-Darcian water flow in clay. J. Hydrol. 430, 173–178.
Loucks, R.G., Reed, R.M., Ruppel, S.C., Jarvie, D.M., 2009. Morphology, genesis, and distribution of nanometer-scale pores in siliceous mudstones of the Mississippian Barnett Shale. J. Sed. Res. 79 (12), 848–861.
Lu, F., Yang, J., Kwok, D.Y., 2004. Flow field effect on electric double layer during streaming potential measurements. J. Phys. Chem. B 108 (39), 14970–14975.
Masliyah, J.H., Bhattacharjee, S., 2006. Electrokinetic and colloid transport phenomena. John Wiley & Sons.
Miller, R.J., Low, P.F., 1963. Threshold gradient for water flow in clay systems 1. Soil Sci. Soc. Am. J. 27 (6), 605–609.
Mitsoulis, E., 2007. Flows of viscoplastic materials: models and computations. Rheol. Rev. 2007, 135–178.
Multiphysics, C., 2012. Comsol multiphysics user guide (version 4.3 a). COMSOL, AB: 39-40.
Papanastasiou, T.C., 1987. Flows of materials with yield. J. Rheol. 31 (5), 385–404.
Prada, A., Civan, F., 1999. Modification of Darcy's law for the threshold pressure gradient. J. Petrol Sci. Eng. 22 (4), 237–240.
Rand, B., Melton, I.E., 1977. Particle interactions in aqueous kaolinite suspensions: I. Effect of pH and electrolyte upon the mode of particle interaction in homoionic sodium kaolinite suspensions. J. Colloid Interface Sci. 60 (2), 308–320.
Rice, C., Whitehead, R., 1965. Electrokinetic flow in a narrow cylindrical capillary. J. Phys. Chem. 69 (11), 4017–4024.
Shashikumar, N., Gireesha, B., Mahanthesh, B., Prasannakumara, B., Chamkha, A.J., 2019. Entropy generation analysis of magneto-nanoliquids embedded with aluminium and titanium alloy nanoparticles in microchannel with partial slips and convective conditions. Int. J. Numer. Meth. Heat Fluid Flow.
Soni, J., Islam, N., Basak, P., 1978. An experimental evaluation of non-Darcian flow in porous media. J. Hydrol. 38 (3–4), 231–241.
Swartzendruber, D., 1962a. Modification of Darcy's law for the flow of water in soils. Soil Sci. 93 (1), 22–29.
Swartzendruber, D., 1962b. Non-Darcy flow behavior in liquid-saturated porous media. J. Geophys. Res. 67 (13), 5205–5213.
Tang, G., Wang, S., Ye, P., Tao, W., 2011. Bingham fluid simulation with the incompressible lattice Boltzmann model. J. Nonnewton. Fluid Mech. 166 (1–2), 145–151.
Torrance, J.K., 1999. Physical, chemical and mineralogical influences on the rheology of remoulded low-activity sensitive marine clay. Appl. Clay Sci. 14 (4), 199–223.
Wang, F., et al., 2009. Influence of wettability on flow characteristics of water through microtubes and cores. Chin. Sci. Bull. 54 (13), 2256–2262.
Wang, J., Wang, M., Li, Z., 2006. Lattice Poisson-Boltzmann simulations of electro-osmotic flows in microchannels. J. Colloid Interface Sci. 296 (2), 729–736.
Wang, X., Sheng, J.J., 2017. Effect of low-velocity non-Darcy flow on well production performance in shale and tight oil reservoirs. Fuel 190, 41–46.
Wei, X., Qun, L., Shusheng, G., Zhiming, H., Hui, X., 2009. Pseudo threshold pressure gradient to flow for low permeability reservoirs. Pet. Explor. Dev. 36 (2), 232–236.
Wu, J., et al., 2017a. Experimental study of nonlinear flow in micropores under low pressure gradient. Transport Porous Med. 119 (1), 247–265.
Wu, J., et al., 2017b. Flow of Newtonian fluids with different polarity in micro scale. Chin. Sci. Bull. 62 (25), 2988–2996.
Xue-wu, W., Zheng-ming, Y., Yu-ping, S., Xue-wei, L., 2011. Experimental and theoretical investigation of nonlinear flow in low permeability reservoir. Procedia Environ. Sci. 11, 1392–1399.
Yang, L., Qun, L., Xiangui, L., Hanmin, X., 2011. Characteristics of micro scale nonlinear filtration. Pet. Explor. Dev. 38 (3), 336–340.
Zeng, B., Cheng, L., Li, C., 2011. Low velocity non-linear flow in ultra-low permeability reservoir. J. Petrol Sci. Eng. 80 (1), 1–6.
Zhang, L., Wang, M., 2015. Modeling of electrokinetic reactive transport in micropore using a coupled lattice Boltzmann method. J. Geophys. Res. Solid Earth 120 (5), 2877–2890. https://doi.org/10.1002/2014JB011812.
Zhang, W., Yao, J., Sun, H., 2015. Electrokinetic coupling in single phase flow in periodically changed capillary with a very small throat size. Int. J. Heat Mass Transfer 84, 722–728.
Zhang, X., et al., 2019. Microscale effects of Bingham-plastic liquid behavior considering electroviscous effects in nano-or microsized circular tubes. Phys. Fluids 31 (2), 022001.
Zhao, H., et al., 2015. Petrophysical characterization of tight oil reservoirs using pressure-controlled porosimetry combined with rate-controlled porosimetry. Fuel 154, 233–242. https://doi.org/10.1016/j.fuel.2015.03.085.
Zhu, W., Tian, Y., Yu, M., 2014. Mechanism of microscopic fluid flow in microtubes. Sci. Technol. Rev 32 (27), 23–27.